Chair of Technical Thermodynamics | RWTH AACHEN UNIVERSITY

The present work was submitted to Chair of Technical Thermodynamics

Environmental optimization of the recovery and utilization of steel mill off-gases in the chemical industry

Masterthesis

presented by
Leitl, Matthias
StudentID no. 345972

Supervisor:
Johanna Kleinekorte, M.Sc.

1^{st} Examiner: Univ.-Prof. Dr.-Ing. Niklas von der Aßen
2^{nd} Examiner: Raoul Meys, M. Sc.

Aachen, September 8, 2020

Abstract

The global steel and chemical industry contribute largely to industrial greenhouse gas (GHG) emissions. While the emissions of the steelmaking process are related to off-gases, the emissions of chemical production are related to the consumption of fossile fuels. When separated from steel mill off-gases, carbon dioxide and other gas components can be utilized as feedstock for chemical production, consequently reducing fuel consumption and emissions. In the present work, we determine optimal utilization pathways for steel mill off-gases and investigate the GHG reduction potential of the separation system. We combine a non-linear, disjunctive model of the separation system and a large-scale linear model of the chemical industry to perform environmental optimization. Through the integrated approach, interactions between both sub-systems are captured. The optimal utilization of steel mill off-gases, and hence the optimal design of the separation system, depend on the carbon footprint of electricity. For current high and moderate footprints, methane, hydrogen and synthesis gas can be recovered as feedstocks for conventional chemical production. For low electricity footprints in the future, the separation system promotes CO_2-based production processes in the chemical industry, supplying up to 30% of the required CO_2. By coupling the global steel and chemical industry, industrial GHG emissions can be reduced by 80 Mt CO_2-equivalents per year.

Contents

List of Figures

List of Tables

1. Introduction

Reducing green house gas (GHG) emissions to prevent global warming is one of the major challenges for the next decades. Industrial carbon dioxide (CO_2) emissions account for significant shares of the anthropogenic GHG emissions and are accordingly in the focus of attention. In particular, the global steel and chemical industry represent two main emitters. Reducing fossil fuel consumption through process intensification led to a steady decline of emissions. Recently, this gradual improvement decelerated as thermodynamical limits are approached. Utilization of fossil carbon feedstocks in the chemical industry and fossil reducing agents in the steelmaking process represent main obstacles for further improvement. To overcome this limitations, breakthrough innovations are required [1].

Among several technologies for the production of steel from iron ore, the integrated route is most significant. As first step of the integrated route, coal is pyrolized to coke in the coke oven. The central reactor of the steelmaking process is the blast furnace. Coke and iron ore are fed into the blast furnace and exposed to air at high temperatures. By reducing and melting, liquid iron with high carbon content is produced. As reduction takes place and energy is supplied for heating, the blast furnace is the greatest emission source in steelmaking. To obtain steel, the carbon content of the melt must be decreased. Accordingly, the last step of the integrated route is conducted. In the basic oxygen furnace, oxygen is blown onto the liquid iron. Carbon and other elements react with oxgygen and are thereby removed from the melt. [2]

All three process steps emit off-gases, which are referred to as steel mill off-gases and differ in quantity and composition. Largest stream is the Blast Furnace Gas (BFG), containing carbon monoxide (CO) and CO_2 as result of the reduction process. Furthermore, nitrogen (N_2) is most present in this gas stream due to the reaction with air. In contrast to BFG, the basic oxygen furnace gas (BOFG) is almost nitrogen free. The third off-gas stream, coke oven gas (COG), contains mainly hydrogen (H_2) and methane (CH_4). Figure 1.1 shows the molar composition of the steel mill off-gas streams.

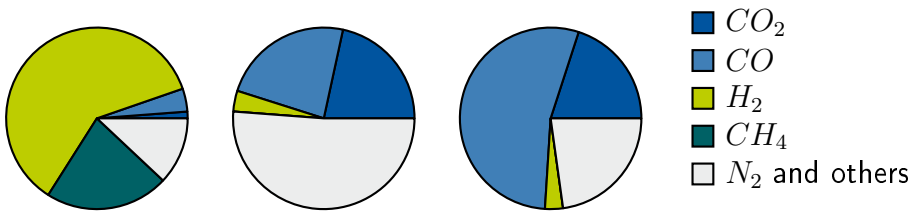

Figure 1.1.: Chemical composition of steel mill off-gas streams (mole fractions). Coke oven gas (COG, left), blast furnace gas (BFG, center) and basic oxygen furnace gas (BOFG, right)

Due to the presence of combustible components (H_2, CH_4 and CO), the three off-gas streams have elevated heating values. Therefore, thermal utilization is currently performed. The steel mill off-gases are combusted, either for reheating processes inside the steel mill or to generate power [2]. However, thermal utilization converts all carbonated components to CO_2, causing direct GHG emissions. Recently, several authors presented alternative utilization pathways. Using steel mill off-gases for the recovery of valuable components and the synthesis of chemical products is referred to as chemical utilization. Methanol and dimethyl ether are two proposed products of chemical utilization pathways. Furthermore, polygeneration systems can combine chemical and thermal utilization, producing both energy and chemicals [6, 7, 27].

As most chemical products contain carbon, the chemical industry inevitably depends on carbon feedstocks. Today, the chemical industry contributes significantly to industrial GHG emissions by consuming fossile fuels. Carbon capture and utilization (CCU) represents an alternative carbon feedstock. CO_2 is captured and converted to chemical products, thereby avoiding emissions. Two different types of sources are applicable for CCU. First, CO_2 can be separated from ambient air (direct air capture). Second, industrial point sources can be deployed. Power plants, ammonia plants and steel mills represent main industrial CO_2 sources [25]. In addition, many CCU-based production pathways require H_2 as co-reactant for the inert CO_2 [15]. Environmentally beneficial hydrogen sources are therefore inevitable.

Steel mill off-gases contain significant amounts of CO_2 and H_2. Accordingly, connecting steel and chemical industry via chemical steel mill off-gas utilization is promising in order to cut industrial GHG emissions. However, the utilization of gas mixture components requires previous separation. Energy is required to conduct these separation steps. Supplying heat and electricity causes indirect GHG emissions, mitigating the overall reduction potential.

The scope of interest consequently involves the steel industry, the chemical industry and the separation system. In the present work, we perform environmental optimization on this polygeneration system. Interactions between the sub-systems are captured through the integrated approach. Three research questions arise with regard to the intoduced topic: First, *what is the optimal utilization pathway for steel mill off-gases?* Second, *what is the optimal process design for the separation system?* Third, *in which magnitude does steel mill off-gas separation affect the GHG reduction potential of the polygeneration system?*

2. Theoretical Background

To perform environmental optimization, we require a method to evaluate and optimize the eco-friendlieness of production pathways. Life cycle assessment and the Technology Choice Model accomplish this task (see Section 2.1). In Section 2.2, we introduce the basic unit operations for steel mill off-gas separation. Subsequently, we present generalized disjunctive programming as mathematical approach to aggregate the separation system.

2.1. Life Cycle Assessment and the Technology Choice Model

Life cycle assessment (LCA) is a holistic approach to evaluate the environmental impact of processes and products. The assessment is conducted on the basis of different impact categories, such as global warming impact (GWI) or fossil fuel depletion. Several phases of the product life cycle are evaluated. In this context, cradle-to-gate refers to the impact of raw material supply and production process, while cradle-to-grave evaluation also considers use phase and disposal of the product [29].

To perfom the LCA, we require data about inputs and outputs of the evaluated processes. This data is collected and aggregated in the life cycle inventory (LCI). Between the processes $j \in \{1, \ldots, n\}$ of the production system, intermediate flows $i \in \{1, \ldots, m\}$ are exchanged. Several commodities are considered as intermediate flows, including utilities such as heat, energy and process water as well as chemical products or waste. The technology matrix $A^{n \times m}$ quantifies the system, as the coefficients a_{ij} indicate the amount of flow i produced ($a_{ij} > 0$) or consumed ($a_{ij} < 0$) by process j. Equation 2.1 shows the structure of the technology matrix [12].

$$\mathbf{A} = \underbrace{\left.\begin{pmatrix} a_{11} & \cdots & \cdots & \cdots & a_{1n} \\ \vdots & \ddots & & & \vdots \\ \vdots & & a_{ij} & & \vdots \\ \vdots & & & \ddots & \vdots \\ a_{m1} & \cdots & \cdots & \cdots & a_{mn} \end{pmatrix}\right\} m \text{ intermediate flows}}_{n \text{ processes}} \tag{2.1}$$

All processes are combined in such a way, that the final demand y_i for each intermediate flow is met. In the resulting linear equation system, the scaling vector $s \in R^n$ characterizes such a solution (see Equation 2.2). For every process, the coefficient s_j indicates in which quantitity process j is conducted.

$$As = y \tag{2.2}$$

The impact vector h contains the environmental impact of the solution in the different categories. These impacts are influenced by several environmental flows, denoted for each process in the elementary flow matrix B. Through the characterization matrix Q, the impact vector h is calculated:

$$h = QBs \tag{2.3}$$

In the following, the GWI is considered as single impact category. Furthermore, only CO_2 is exchanged with the atmosphere as environmental flow. This eliminates the characterization matrix ($Q = 1$) and simplifies B to the emission vector b. Each element b_j represents the CO_2-emssions of a process. The simplified approach allows to rate the eco-friendlieness of the solution with an one-dimensional indicator.

Usually, more than one production route is available for each product ($n > m$). Accordingly, the linear equation system is underdetermined and has more than one solution [5]. The Technology Choice Model (TCM) applies linear programming (LP) on LCI data [14]. The optimization of the scaling vector s provides the most environmental beneficial process system. In this work, the objective function z represents the GWI. The linear equation system (Equation 2.2) is retained as set of constraints. Equation 2.4 shows the TCM in the LP standard form.

$$\begin{aligned} \min_{s} \quad & z = b^T s \\ \text{s.t.} \quad & As = y \\ & s \geq 0 \end{aligned} \tag{2.4}$$

The TCM allows to examine a variety of possible production and utilization pathways for each intermediate flow. Accordingly, the TCM is used to model large-scale production systems, such as the chemical and fuel industry [15]. On industry scale, the linear model equations of the TCM reproduce reality with sufficient accuracy. Furthermore, this formulation allows to use linear optimization solvers, leading to fast and robust solutions. However, for the in-depth investigation of smaller sub-systems, linear models may not suffice. A separation system for steel mill off-gases represents such a non-linear sub-system. By adding the non-linear sub-model to the linear TCM, advantages of both modelling approaches could be combined. However, NLP solvers are required to solve this integrated model. The present work investigates whether the integration affects the ability of fast and robust solution.

2.2. Unit Operations for the Separation System

All three steel mill off-gases are mixtures of different chemical components. The separation of these gas mixtures is inevitable for the subsequent chemical utilization of single components. Successive separation steps are carried out to recover the valuable components, including H_2, CO and CO_2. In the following section, we present unit operations for these separation steps. Absorption and adsorption processes are among those unit operations. The target component is selectively removed from the gas mixture through chemical or physical binding. While absorption refers to the transfer into a liquid solvent, adsorption refers to the interaction at a solid surface. Both mechanisms prefer low temperatures and high pressures. In the subsequent desorption step, the binding is repealed and the target component is recovered in gaseous state. Respectively, high temperatures and low pressures are favorable for desorption. Additionally, chemical reactions are performed to convert the components. Thoses reactions cover the reforming of CH_4 and the conversion of CO to CO_2 and H_2.

2.2.1. Pressure Swing Adsorption

Pressure swing adsorption (PSA) exploits the pressure dependency of the adsorption equilibrium. The adsorption step is performed at high pressure levels. Through transfer at the solid material (adsorbent) surface, target component is removed from the gas mixture. Compressing the feed gas stream requires energy. Accordingly, the feed compressor power is the main energy cost of the process. The desorption step is conducted subsequently. By lowering the pressure, the target component leaves the adsorbent surface and is recovered in gaseous state [8].

Continuous operation of the PSA process requires a certain unit arrangement, as seen in Figure 2.1. The circulation of the adsorbent between two pressure levels is hard to conduct. Instead, the adsorbent bed is fixed in two columns. The continous PSA is operated in two cycles. Switching between the cycles requires several valves. Only one column at a time is connected to the feed and by-product stream, therefore representing the adsorption column. In the fixed adsorbent bed of column 1, the target component accumulates. When the adsorbent is saturated, column 1 is disconnected from feed and by-product stream and connected to the product stream. Now, the desorption step takes place in column 1. The respective opposite step occurs simultaneously in the column 2 [17].

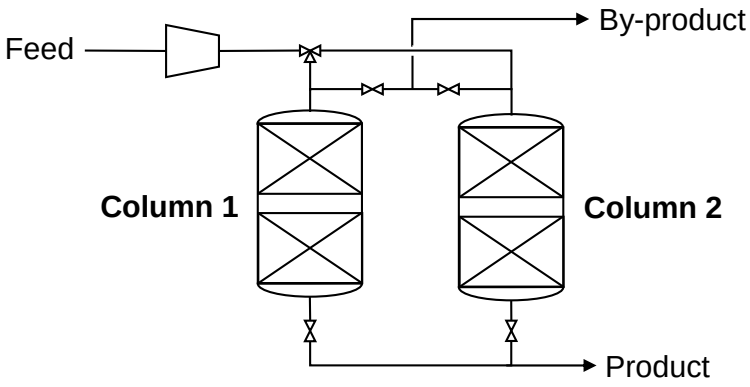

Figure 2.1.: Basic flowsheet of the continous pressure swing adsorption process (PSA)

The PSA process is suitable for two tasks is steel mill off-gas separation: First, the recovery of H_2 from COG, BFG and BOFG [6, 27]. Second, the recovery of CO_2 from BFG and BOFG. Kim et al. [16] presented a detailed study on the application of PSA to recover CO_2 from steel mill off-gas streams.

2.2.2. Temperature Swing Adsorption

Temperature swing adsorption (TSA) exploits the temperature dependency of the adsorption equilibrium. The adsorption step is performed at moderate temperatures. For the desorption step, the temperature is increased. Subsequently, the target component is released. Heating up the product-enriched adsorbent is the greatest operational energy requirement of this process [8]. Ghanbari et al. [7] suggested TSA for the recovery of CO from BFG and BOFG. Rabo et al. [22] investigated the adsorption behaviour of CO at zeolitic molecular sieves. While the adsorption process showed a strong temperature dependency, no significant pressure dependency was observed. Accordingly, TSA was found suitable for CO recovery.

2.2.3. Chemical Absorption

The main concept of chemical absorption is the transfer of the gaseous target component into a liquid solvent (absorbent). Chemical reactions take place in the liquid phase, thereby retaining the target component. In the subsequent desorption step, the reactions are reversed. The target component is stripped from the solvent and recovered as gaseous product.

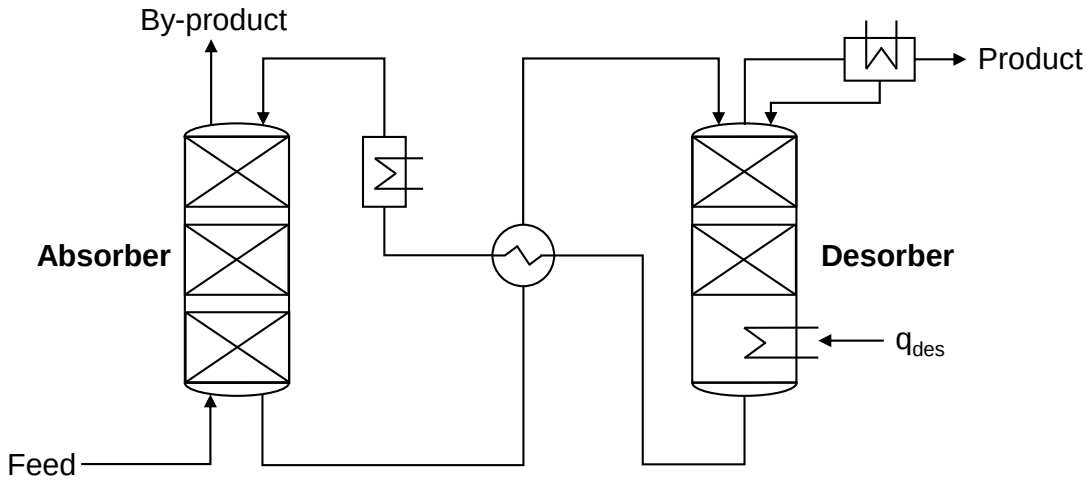

Figure 2.2.: Basic flowsheet of the chemical CO_2 absorption process (CCA)

Carbon chemical absorption (CCA) with aqueous monoethanolamine (MEA) solutions is the conventional set-up for removing CO_2 from gas streams. Figure 2.2 shows the main units of this separation process. The absorber is operated at temperatures around 40°C. The lean solvent enters at the top and flows countercurrent to the feed gas stream through the column. The product-enriched solvent is drained at the bottom and sent to the desorber. As the desorption step takes place at elevated temperatures (around 120°C), the rich solvent is pre-heated by the lean solvent stream leaving the desorber. Main energy cost of the CCA process is the desorption heat, supplied in the desorber bottom. Because of the elevated temperatures, water evaporates from the MEA solution. To obtain a pure product, this water is removed from the product gas stream in a condenser at the column top [16, 21].

2.2.4. Membrane Separation Process

Membrane separation processes (MSPs) are investigated as alternative to the conventional gas separation processes. Key element is the membrane, beeing selectively permeable to the target component. The feed gas stream enters the membrane module at elevated pressure and flows along the membrane. By passing through the membrane, the product stream (permeate) enriches with the target component. The by-product stream (retentate) leaves the module without passing the membrane. Lower energy requirements are the most prominent advantage of MSPs [8]. However, limited product purities are the main drawback [16]. To obtain a product stream of sufficient quality, multiple membrane stages are required. Moreover, purity and product recovery form a trade-off. Higher feed pressures force more gas through the membrane, increasing the product recovery rate. At the same time, the product purity decreases [27].

Two steps in the separation of steel mill off-gases can be conducted with MSPs: First, the recovery of H_2 from COG, BFG and BOFG. Second, the recovery of CO_2 from BFG and BOFG [7, 27]. Lie et al. [18] presented a detailed study on the recovery of CO_2 from steel mill off-gases with a fixed site carrier membrane.

2.2.5. Water Gas Shift Reaction

The water gas shift reaction (WGSR) enhances the flexibility of the separation system: Under addition of steam (H_2O), CO is converted into H_2 and CO_2 by the equilibrium reaction (see Equation 2.5). Thereby, the ratio of the three products is adjusted to fulfill the demands of the subsequent utilization. The reaction enthalpy is denoted by ΔH_R.

$$\mathrm{CO} + \mathrm{H_2O} \rightleftharpoons \mathrm{CO_2} + \mathrm{H_2} \qquad \Delta H_R = -41.1\ kJ/mol \tag{2.5}$$

According to Le Chatelier's principle, low temperatures raise the equilibrium product concentration of the exothermic reaction. However, the reaction decelarates at low temperatures. To adress this trade-off between kinetics and equilibrium, several operation modes are applied. For the WGSR of steel mill off-gases, the low-temperature shift reaction (LTSR) was found promising. The LTSR is operated at 200 - 300 $°C$ over Cu-Zn catalysts. High conversion rates are achieved for a molar H_2O to CO ratio of at least one [4].

2.2.6. Methane Reforming

Methane reforming decomposes CH_4 into H_2 and CO. Many chemical production processes consum this product mixture, referred to as synthesis gas (SynGas). The ratio between both components varies for each process and is therefore an important property. SynGas 2:1 denotes a molar H_2-to-CO-ratio of 2:1. Three different reaction steps can be applied to methane reforming:

Steam methane reforming

Steam methane reforming (SMR) is the conventional reaction step. However, the strong endothermic SMR involves the drawback of significant heat consumption. The product mixture contains comparatively high amounts of H_2, resulting in SynGas 3:1 (see Equation 2.6). Simultaneos to the SMR, the WGSR takes place.

$$\mathrm{CH_4 + H_2O \rightleftharpoons CO + 3\,H_2} \qquad \Delta H_R = 234.7\ kJ/mol \tag{2.6}$$

Partial oxidation reforming

Partial oxidation reforming (POR) is slightly exothermic and therefore beneficial in terms of energy consumption. However, the reaction requires pure oxygen (O_2) as co-reactant (see Equation 2.7). Additional costs are related to the oxygen supply. SynGas 2:1 is obtained as product stream, the optimal composition for most subsequent production processes [33].

$$\mathrm{CH_4 + 0.5\,O_2 \rightleftharpoons CO + 2\,H_2} \qquad \Delta H_R = -35.9\ kJ/mol \tag{2.7}$$

Carbon dioxide reforming

Carbon dioxide reforming (CDR) utilizes CO_2 as co-reactant. Therefore, CDR is considered as CCU technology. Heat is supplied to perform the strongly endothermic reaction step. SynGas 1:1 is produced, according to the stoichiometry (see Equation 2.8) [31].

$$\mathrm{CH_4 + CO_2 \rightleftharpoons 2\,CO + 2\,H_2} \qquad \Delta H_R = 247\ kJ/mol \tag{2.8}$$

2.3. Generalized Disjunctive Programming

In the present work, we intend to determine the optimal steel mill off-gas separation system. Aggregating this system incorporates two tasks, referred to as conceptual process design: first, the selection of unit operations and their connectivity; second, the selection of operating points. Superstructure optimization is a methodical approach to this challenge. The superstructure contains all interesting process alternatives, hence incorporating all possible flowsheet configurations. Through mathematical optimization of the superstructure, the optimal flowsheet is found. Transforming the superstructure into a mathematical formulation is challenging [20]. Both continous model variables and discrete design decisions are involved. In most cases, the model includes non-linear equations. Mixed integer non-linear programming (MINLP) is the conventional formulation for superstructure optimization problems. Design decisions are represented by integer variables, which are often binary. However, MINLP formulations of superstructure models are not unique. Several formulations can be found for the same problem [9].

Generalized Disjunctive Programming (GDP) is an alternative approach for the formulation of superstructure optimization problems. By representing desing decisions through logical connectors, the GDP formulation is unique for each problem. The general form of a GDP [23] is shown in Equation 2.9:

$$\min \quad z = f(x) \qquad x \in \mathbb{R}^n \tag{2.9a}$$

$$\text{s.t.} \quad g(x) \leq 0 \tag{2.9b}$$

$$\vee_{i \in D_k} \begin{bmatrix} Y_{ki} \\ r_{ki}(x) \leq 0 \end{bmatrix} \qquad k \in K \tag{2.9c}$$

$$\veebar_{i \in D_k} Y_{ki} \qquad Y_{ik} \in \{True, False\} \tag{2.9d}$$

$$\Omega(Y) = True \tag{2.9e}$$

The objective function z depends only on the continuous model variables x. Global constraints $g(x)$ cover equalities and inequalities of the model that are always enforced, independent of the discrete realizations. On the contrary, disjuncts represent model alternatives that may or may not be selected. Each disjunct i consists of a constraint set r_{ki} and a boolean indicator variable Y_{ki} (see 2.9c). If the disjunct is active, Y_{ki} is $True$ and r_{ki} is enforced. If i is not active, Y_{ki} is $False$ and r_{ki} is ignored. The disjunctions k represent logical or-connections between the disjuncts: Always exactly one disjunct of each disjunction is selected. Here, the exclusive-or operator is denoted by $\veebar$ (2.9d). In addition, logical constraints $\Omega(Y)$ can be formulated with propositional logic between the disjuncts. For example, the selection of one disjunct leads to the selection of another disjunct [9].

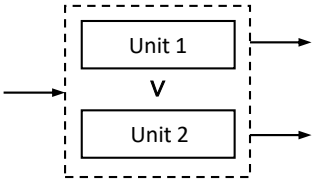

Figure 2.3.: Graphical representation of a disjunction in the superstructure

Applied to process engineering, the disjuncts refer to unit or process alternatives. While r_{ki} contains all model equations of unit i, the indicator variable Y_{ki} denotes the existence of i in the final flowsheet, hence the optimal solution. The disjunction k represents the design decision between several alternatives for the process task. Figure 2.3 shows the graphical representation of this correlation in the superstructure flowsheet.

Two strategies are used to solve optimization problems in GDP formulation: First, transform the GDP into MINLP formulation. Subsequently, established MINLP solvers can be applied. Second, solve the GDP directly with a logic-based solver. Recently, GDPopt [3] was introduced as direct solver. In the present work, we use GDPopt to solve the disjunctive overall model.

3. Method: Non-linear Extension of the Technology Choice Model

In the present work, we combine the sub-models of the chemical industry and the separation system to an integrated model. Through this approach, mutual interactions between the sub-systems affect the optimal solution. In particular, we investigate how the optimal design of the separation system changes to meet the demands of the chemical industry. Previous studies used the TCM to analyze the chemical industry [15]. Linear processes characterize the model, exchanging mass and energy flows. For industry-scale processes, this problem formulation provides reasonable accuracy. In constrast, we require a more detailed model for the separation system, including non-linear equations and discrete design decisions. Accordingly, we present a framework to combine both approaches into one model. The integrated model allows to extend the TCM by non-linear sub-system, while also retaining most of the original formulation. First, we present the stream and unit variables of the flowsheet model (Section 3.1). Subsequently, in Section 3.2, the TCM is modified for the connection of flowsheet streams. In Section 3.3, we introduce overall mass and energy balances to characterize the connection points. Lastly, the objective function of the integrated model is shown in Section 3.4.

3.1. Stream and Unit Variables of the Flowsheet

Each stream i in the flowsheet is characterized by a set of stream variables, including temperature T^i, pressure p^i and molar flow rates n^i. Furthermore, each considered chemical component k is represented by the mole fraction y_k^i. Mole balance equations are applied to all unit operations. Component balances are set up for each chemical component. For one component per stream, the component balance is replaced by the closure condition:

$$1 = \sum_k y_k^i \tag{3.1}$$

For separation processes, the product recovery $\zeta_{k_{\text{prod}}}$ indicates, which share of the product component k_{prod} in the feed n^{in} is recovered in the product stream n^{prod} (see Equation 3.2). Energy balances and shortcut equations are used to determine the main energy requirements. A detailed outline of these equations for the separation system can be found in Appendix B.

$$\xi_{k_{\text{prod}}} = \frac{n^{\text{prod}} y_{k_{\text{prod}}}^{\text{prod}}}{n^{\text{in}} y_{k_{\text{prod}}}^{\text{in}}} \tag{3.2}$$

Splitters divide the input stream n^{in} into two output streams ($n^{\text{out},1}$ and $n^{\text{out},2}$). The flow ratio between both output streams depends on the split factor $\xi^{\text{out},i}$, referred to one of the output streams (Equation 3.3). Molar composition, temperature and pressure are equal for the three streams.

$$\xi^{\text{out},1} = \frac{n^{\text{out},1}}{n^{\text{in}}} \tag{3.3}$$

Chemical reactors are modelled with one input and one output stream. The conversion rate ζ_R describes, which share of the limiting component k_{key} is converted into product (Equation 3.4). The detailed balance equations for reactors are shown in Appendix B.

$$\zeta_R = 1 - \frac{n^{\text{out}} y_{k_{\text{key}}}^{\text{out}}}{n^{\text{in}} y_{k_{\text{key}}}^{\text{in}}} \tag{3.4}$$

3.2. Modified Technology Choice Model

The integrated model adopts equations and variables of the TCM. However, certain streams of the flowsheet interact with the linear TCM model. For instance, CCU processes utilize gas components from the separation system. To capture these interactions with the integrated model, we modify the equations of the TCM. Furthermore, we use production volumes to quantify chemical production. Accordingly, the modifications of the TCM involve:

- Elementwise notation
- Production volumes for chemical products
- Connection to the separation system

In accordance to the matrix form of Equation 2.4, we define the final demand y_i elementwise for each intermediate flow:

$$y_i = \sum_{j=1}^{n} a_{ij} s_j \qquad i \in \{1, \dots, m\} \tag{3.5}$$

Instead of setting the final demand, we introduce production volumes $p_i > 0$ for the products of the chemical industry [15]. Accordingly, the following volume constraints are enforced for each product:

$$\sum_{j=1}^{n} a_{ij}^{+} s_j - p_i \geq 0 \tag{3.6a}$$

$$a_{ij}^{+} = \begin{cases} a_{ij} & \text{for } a_{ij} > 0 \\ 0 & \text{for } a_{ij} \leq 0 \end{cases}$$

$$y_i \geq 0 \tag{3.6b}$$

The coefficients a_{ij}^{+} indicate positive entries of the technology matrix A, referring to production processes of i. These processes are carried out in such a way, that the production volume is met or exceeded (Equation 3.6a). Furthermore, the consumption of a chemical product must not exceed its production (Equation 3.6b).

Through this approach, we divide the intermediate flows into production chemicals ($p_i > 0$) and supplements ($p_i = 0$). Supplements include energy, water, waste and feedstocks. For chemical products, we enforce the volume constraints (Equation 3.2). For supplements, we enforce the demand constraints of the original TCM (Equation 3.7). The production of each supplement equalizes consumption and disposal:

$$y_i = 0 \tag{3.7}$$

In addition, we consider the flows of the separation system. Accordingly, we introduce connectors c_i for intermediate flows occuring in both sub-models. For supplements consumed by the separation system, including heat and electricity, the connectors take negative values. For supplements produced by the separation system, including CO and H_2, the connector takes postive values. The connectors are added to the demand constraints, as seen in Equation 3.8. Note that production chemicals are neither produced, nor consumed by the separation system. Accordingy, no connectors are added to the volume constraints (Equation 3.2).

$$y_i + c_i = 0 \tag{3.8}$$

While the scaling variable s_j is positive for every process (see Equation 2.4), the final demand variable y_i may take negative values. For supplements generated in the separation system, the respective connector is positive. Accordingly, the final demand must be negative to fulfill the demand constraint.

3.3. Overall Balances

In the previous section, we add connectors to the linear TCM constraints. Hence, we allow interaction of the modified TCM with other sub-models. However, the connectors are not yet quantified. To relate each connector to the respective streams of the separation flowsheet, we establish overall balance equations. All energy flows of the separation system are aggregated and added to the respective overall balance, shown for the electricity flows $w^{i_{\text{el}}}$ ($i_{\text{el}} \in \{1, \dots, m_{\text{el}}\}$) in Equation 3.9. For each chemical component k, we include all product ($i_{\text{prod},k} \in \{1, \dots, m_{\text{prod},k}\}$) and supplement ($i_{\text{in},k} \in \{1, \dots, m_{\text{in},k}\}$) streams of pure k in the balance (Equation 3.10). M_k denotes the molar weight of component k.

$$0 = c_{\text{el}} + \sum_{i_{\text{el}}=1}^{m_{\text{el}}} w^{i_{\text{el}}} \tag{3.9}$$

$$0 = c_k + M_k \left(\sum_{i_{\text{in},k}=1}^{m_{\text{in},k}} n^{i_{\text{in},k}} - \sum_{i_{\text{prod},k}=1}^{m_{\text{prod},k}} n^{i_{\text{prod},k}} \right) \tag{3.10}$$

We consider remains of CO_2 in the waste streams of the separation system as environmental impact. Accordingly, we insert an additional flow category in the LCI (CO_2 to atmosphere) and add the relevant shares of the waste streams ($i_{\text{waste}} \in \{1, \dots, m_{\text{waste}}\}$). In the LCI, the resulting intermediate flow is converted to an environmental flow. Through this procedure, we can penalize varying shares of CO_2 in the waste streams.

$$0 = c_{\text{CO2, to atm}} - M_{CO_2} \sum_{i_{\text{waste}}=1}^{m_{\text{waste}}} n^{i_{\text{waste}}} y_{CO_2}^{i_{\text{waste}}} \tag{3.11}$$

Overall balances are set for all energy forms, chemical components, supplements and waste streams occuring in the separation system. Accordingly, all input and output streams of the flowsheet are connected to the TCM. Linear TCM processes settle the commodities produced or consumed by the separation system. Furthermore, additional demands of certain flows can be considered in the overall balances.

3.4. Objective Function

By using connectors and overall balances, we connect both sub-models of the integrated model. All streams of the flowsheet are connected to the TCM. In particular, all environmental flows of the separation system are settled by the TCM. Thus, the separation system causes no direct GHG emissions. Accordingly, we can use the linear TCM objective function for the integrated model, without any modifications. We consider end-of-life emissions in this linear objective function. Otherwise, the solution tends to store carbon dioxide through excessive chemical production. However, this storage does not improve environmental friendlieness in the long term [15].

$$f(s,y) = \sum_{j=1}^{n} b_j s_j + \sum_{i=1}^{m} v_i y_i \tag{3.12}$$

The first part of the objective function (Equation 3.12) refers to the cradle-to-gate emissions of each process. For the use of CCU technologies, this expression takes very small or even negative values. The second part refers to the end-of-life emissions. We introduce the end-of-life vector v, containing the GHG emissions for the combustion of every considered chemical product.

4. Case Study: Coupling the Global Steel and Chemical Industry

In the following chapter, we present the case study. Figures 4.1 and 4.2 show the system boundaries, hence the scope of the study. All quantities are balanced for the global steel and chemical industry on annual basis. We exclude the steel mills from the model. Accordingly, the steel mill off-gases enter the system as input streams, characterized in Section 4.1. Output of the system are the production volumes of the chemical industry. In the benchmark scenario (see Figure 4.1), the steel mill off-gases are combusted in the power plant to generate heat and electricity. In the polygeneration scenario (see Figure 4.2), we consider combustion and separation as alternatives. Recovered gas components are utilized as feedstock for the chemical industry. Accordingly, we adopt combustion (Section 4.2) and separation (Section 4.3) in the integrated model. In particular, we allow combinations of both pathways. Subsequently, we add the sub-model for the chemical industry, presented in Section 4.4. Then, the integrated model is implemented to perform environmental optimization (Section 4.5).

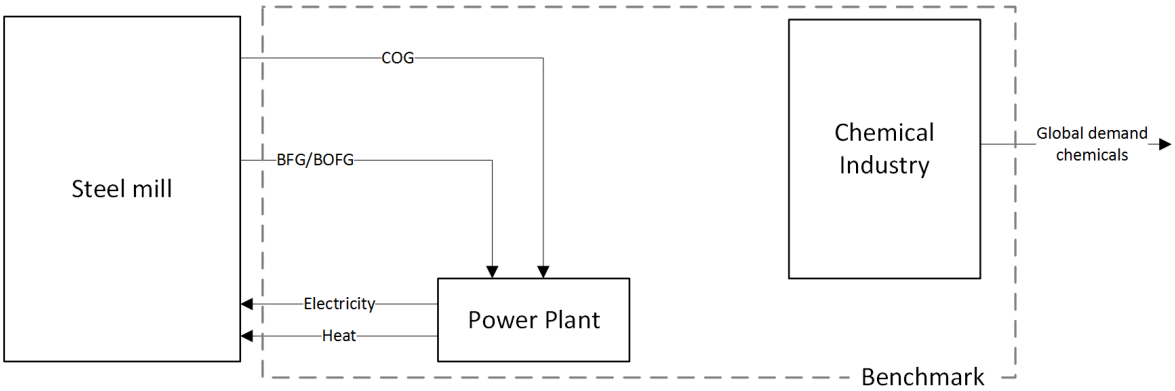

Figure 4.1.: System boundaries of the benchmark scenario

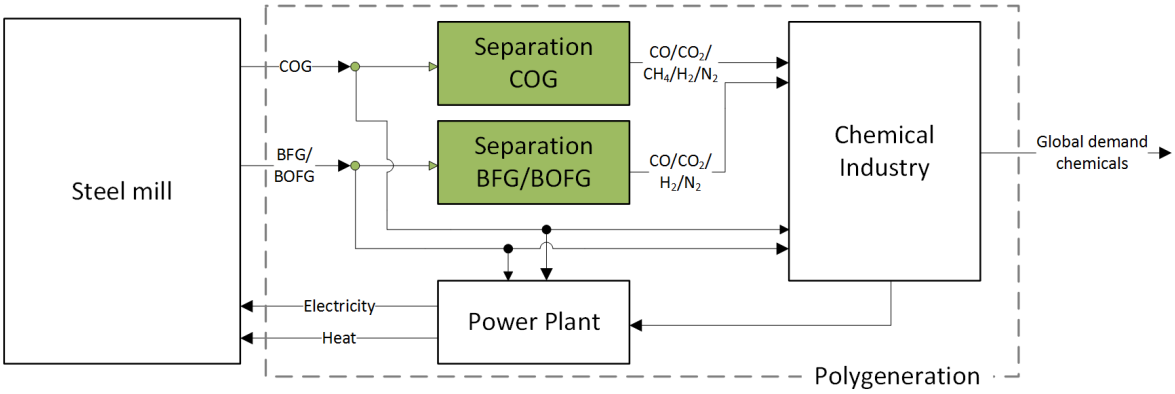

Figure 4.2.: System boundaries of the polygeneration scenario

4.1. Steel Mill Off-Gas Generation

Amount and properties of the generated steel mill off-gases influence the subsequent utilization. However, we exclude steel mills from the integrated model. Instead, the off-gas streams are assumed as stationary. We characterize the respective input stream parameters in Table 4.1. Because of the similar compositions and the low quantity of generated BOFG, we aggregate BFG and BOFG into one stream.

Table 4.1.: Quantity and properties of the annual, worldwide steel mill off-gas streams. Molar compositions are adapted from [27], mass streams are obtained from own calculations.

	in	COG	BFG	BOFG	BFG/BOFG mix
m	Mt/year	39.70	-	-	1740.55
t	°C	30	30	30	30
p	bar	1	1	1	1
M	g/mol	8.94	-	-	30.11
Component k		Mole fractions y_k			
CO_2		0.012	0.22	0.2	0.217
CO		0.042	0.24	0.54	0.25
H_2		0.621	0.04	0.03	0.037
$CH4$		0.225	0	0.3	0
N_2		0.059	0.47	0.18	0.456
H_2O		0.041	0.04	0	0.4

4.2. Combustion Processes

Today, steel mill off-gases are combusted for re-heating and power generation. Accordingly, we include this utilization pathway in the integrated model. As the heat integration of the steel mill is excluded from the model, we consider the combustion in combined heat and power plants (CHP). The linear combustion processes are shown in Table 4.2.

Table 4.2.: Combustion processes for steel mill off-gases [32]

Interm. Flow	in	Combustion BFG/BOFG in CHP	Combustion COG in CHP
BFG/BOFG	kg	-0.370	0
COG	kg	0	-0.027
Electricity	MJ	0.365	0.396
Heat	MJ	0.145	0.145
Water	kg	-0.177	0.206
GWI	kg CO_2-eq	0.263	0.036

When steel mill off-gases are utilized for chemical production, the combustion is discontinued. The resulting demand of heat and electricity is settled from other sources. Accordingly, we consider an annual demand of 248 TWh heat and 638 TWh electricity in the polygeneration system, equalizing the complete combustion of the steel mill off-gas streams in the CHP.

4.3. Separation System

The steel mill off-gas separation system (MGS) is implemented as disjunctive superstructure model. All required unit operations are described in Section 2.2. Stream and unit variables for the model are introduced in Section 3.1. We use a fixed sequence and connectivity of the separation steps, adapted from Ghanbari et al. [7].

The first step of the COG separation (see Figure 4.3) is the H_2 recovery. MSP or PSA are applied for this task. For both pressure-driven units, we require an upstream compressor. The by-product stream contains mainly CH_4, which can either be utilized (Stream 35) or converted. To produce SynGas, Stream 37 supplies the co-reactant (CO_2, H_2O or O_2). Subsequently, the mixture is sent to the methane reforming unit. Three reactions

are applicable to this task: SMR, CDR and POR (see Section 2.2.6). Dependent on the selected reaction, heat is consumed or produced. All three reactions are operated at high conversion rates (see Table B.1). Accordingly, we take output stream 40 as pure SynGas.

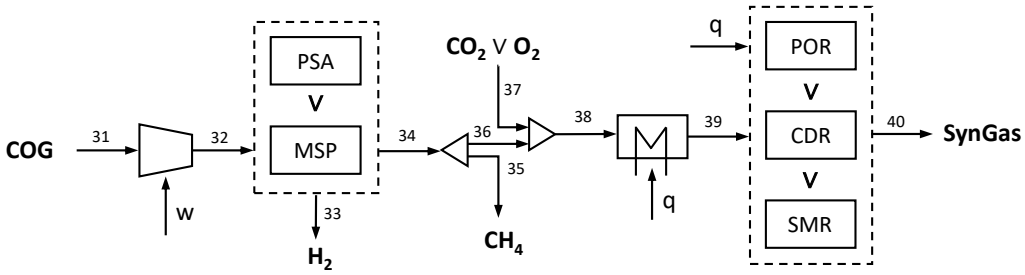

Figure 4.3.: Superstructure of the COG separation system

The BFG/BOFG mixture contains large amounts of CO (see Table 4.1). Thus, we perform CO recovery via TSA as first step (Figure 4.4). Recovered CO is either utilized (Stream 20) or converted. For the WGSR step, steam (H_2O) is supplied as co-reactant (Stream 22). The resulting gas mixture is heated and sent to the reactor. Through the WGSR step, we obtain additional H_2 and CO_2. The reactor output stream (25) is mixed with the TSA by-product stream (4) to conduct further separation.

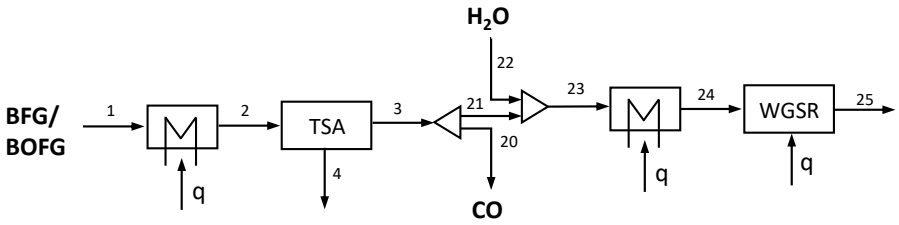

Figure 4.4.: Superstructure of the BFG/BOFG separation system (1/2)

Three unit alternatives can perform the subsequent CO_2 recovery: MSP, PSA or CCA (see Figure 4.5). Through heat exchanger and compressor, we generate the operating conditions for the selected process. Last step of the BFG/BOFG separation is another H_2 recovery step. The by-product stream of this unit (12) contains large amounts of N_2, but also unrecovered gas components. Accordingly, the stream is considered as waste and

passed to the TCM. There, the stream is released to the atmosphere, penalizing shares of environmentally relevant gases, in particular CO and CO_2.

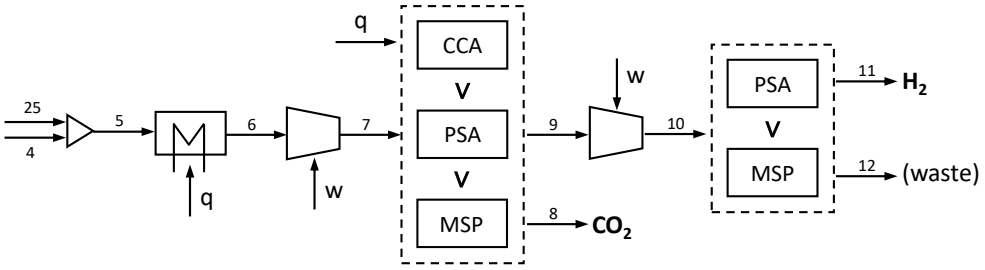

Figure 4.5.: Superstructure of the BFG/BOFG separation system (2/2)

4.4. Chemical Industry

We include 49 relevant chemical products in the model. A complete list of the considered products and the global production volumes is presented in the Appendix (see Table C.1). Furthermore, we incorporate a variety of intermediate chemicals and supplements. The processes of the chemical industry model are available in the LCI notation. Accordingly, we add this sub-model in modified TCM notation to the integrated model.

For each product, we consider conventional production pathways, dependent on fossil fuels. Furthermore, CCU technologies are available for some products. The technology readiness level (TRL) indicates the maturity of a certain process, hence the progress to industrial implementation. In the present work, we exclude low-TRL processes.

Carbon dioxide-based production routes require efficient feedstocks. We adopt three carbon capture processes in the model: First, the recovery from steel mill off-gases. Second, the recovery from ammonia plant off-gas. Third, the direct air capture. The first capture process is modelled in detail as part of the separation system. For ammonia plants and direct air capture, we include linear TCM processes (see Table 4.3).

Table 4.3.: Linear CO_2 capture processes

Interm. Flow	in	Ammonia plant	Direct air capture
Ammonia	kg	1	0
Carbon Dioxide	kg	1.2	1
Electricity	MJ	-0.96	-1.29
Natural Gas	MJ	-32	-4.19
GWI	kg CO_2-eq	0.38	-1

4.5. Building and Solving the Integrated Model

We use Python (Version 3.6) and the Pyomo package [11] to build the integrated model. Pyomo supports object orientated assembling of the optimization program through the `block` class, enabling structured modeling of large systems. Furthermore, several solvers are available through interfaces. The final model consists of 672 constraints, thereof 99 non-linear, and 804 variables. We apply GDPopt [3] to solve the model, using the logic-based outer approximations (LOA) strategy [26]. As NLP sub-solver, we use IPOPT [30]. As MILP sub-solver, we use both glpk and gurobi [10]. As benchmark, we solve the linear TCM without the possibility of separating steel mill off-gases, using glpk and gurobi [10].

5. Results and Discussion

The integrated model combines steel industry and chemical industry as non-linear, disjunctive optimization program. We solve the integrated model for different input parameters. Previous work on the implementation of CCU technologies in the chemical industry indentified the carbon footprint of electricity as important parameter [15]. Based on this consideration, we adress the research questions:

- What is the optimal utilization pathway for steel mill off-gases?
- What is the optimal process design for the separation system?
- In which magnitude does steel mill off-gas separation affect the GHG reduction potential of the polygeneration system?

In Section 5.1, we present results on the optimal steel mill off-gas utilization, hence the partition between separation and combustion. Then, considerations are made on the optimal process design of the separation system (Section 5.2). Furthermore, in Section 5.3, we compare the results of the polygeneration system to reference scenarios. Lastly, we discuss and validate the obtained results (Section 5.4).

5.1. Steel Mill Off-Gas Utilization

In the integrated model, we consider both separation and combustion of steel mill off-gases. Accordingly, combinations of both pathways are possible, producing gases as well as heat and electricity. Unecological separation steps or even the complete separation system can be avoided. In particular, we allow to handle the separation of COG and BFG/BOFG differently. Because of the chemical compositions of both gas streams (see Table 4.1), we expect differences in the respective utilization pathways.

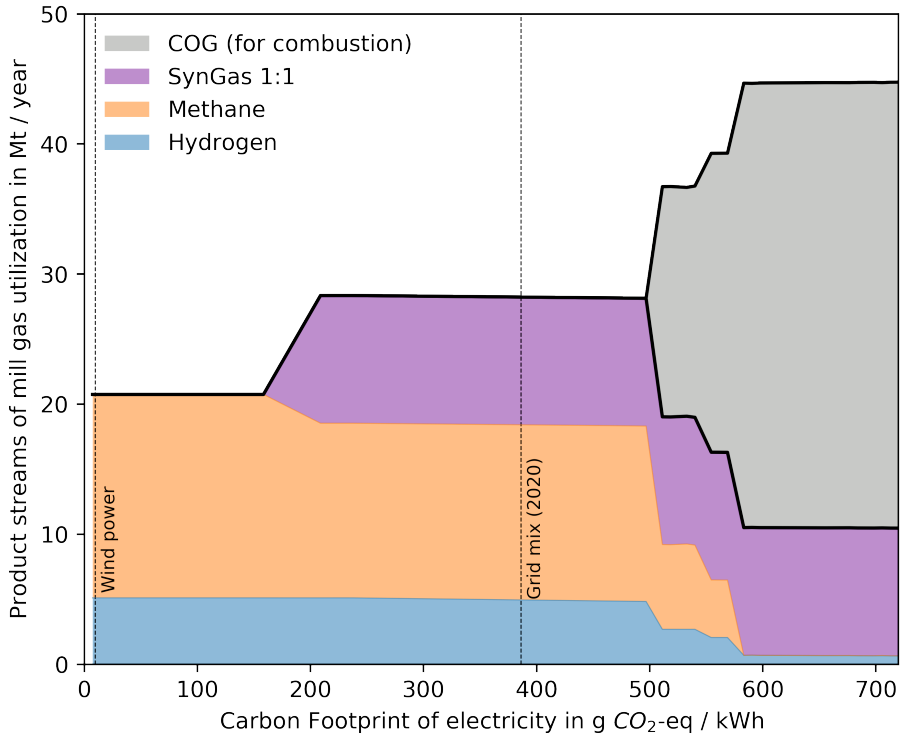

Figure 5.1.: Optimal utilization of COG over the carbon footprint of electricity. Wind: Electricity from wind power (9.57 g CO_2-eq/kWh). Grid mix (2020): Electricity from EU-28 grid mix (386 g CO_2-eq/kWh). Note that the overall mass output of the system changes due to nitrogen purge and reactant supplement.

Figure 5.1 shows the products of the COG separation dependending on the carbon footprint of electricity. Two cases are highlighted: First, the current (2020) EU-28 electricity grid mix (386 g CO_2-eq/kWh) as today's electricity scenario. Second, as theoretical best case, electricity from wind power (9.57 g CO_2-eq/kWh). Generally, due to high H_2 and CH_4 shares, separation is preferred over combustion. Only for carbon footprints over 500 g CO_2-eq/kWh, COG is partly combusted. The product output of the MGS changes between the different electricity scenarios. For today's electricity, a product mix of H_2, CH_4 and SynGas is generated. At lower electricity footprints, we observe a decrease of SynGas production.

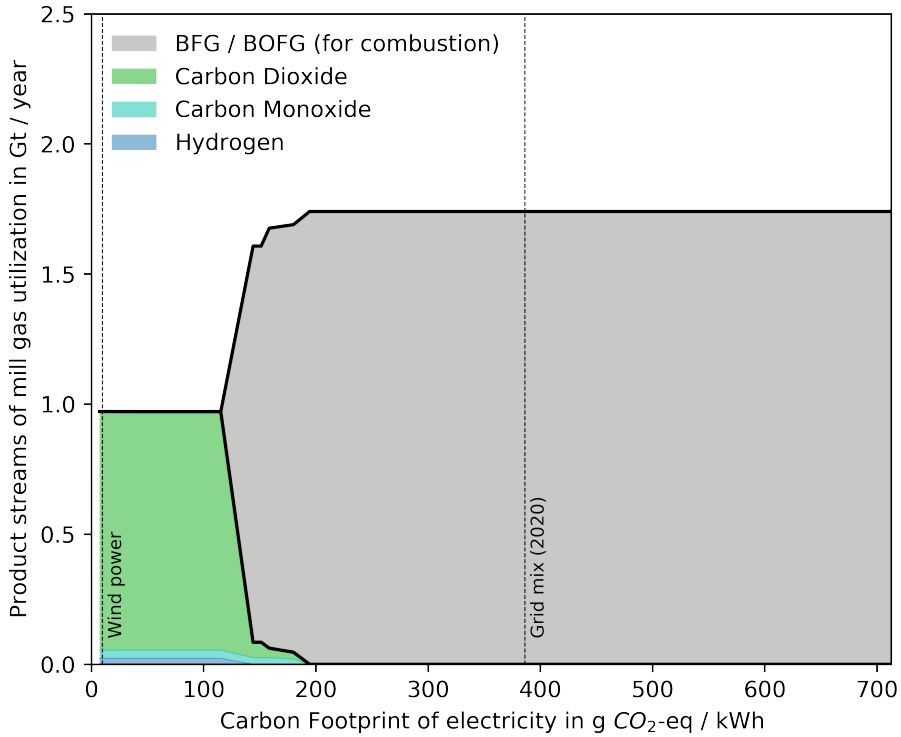

Figure 5.2.: Optimal utilization of BFG / BOFG over the carbon footprint of electricity. Wind: Electricity from wind power (9.57 g CO_2-eq/kWh). Grid mix (2020): Electricity from EU-28 grid mix (386 g CO_2-eq/kWh). Note that the overall mass output of the system changes due to nitrogen purge and reactant supplement.

In contrast to COG, total combustion is the preferred utilization for the BFG/BOFG stream over a wide range of electricity impacts (see Figure 5.2). The BFG/BOFG stream contains large shares of CO and CO_2, and only small shares of H_2. However, we observe a transition at electricity footprints around 200 g CO_2-eq/kWh. Below this point, the BFG/BOFG stream is separated to obtain mainly CO_2, and smaller quantities of CO and H_2. The significant change in utilization is related to the value of CO_2 in the overall system. Decreasing the electricity carbon footprint improves the ecological efficiency of CCU technologies. Accordingly, these technologies replace convential processes, raising the CO_2 demand. Several sources supply CO_2 to fulfill the demand. The share of each source in the overall CO_2 supply depends on the ecological efficiency and, for industrial point sources, on the production limit. First, the most efficient source is exploited. If the demand is not fulfilled, the next sources are selected until enough CO_2 is supplied. In particular, the demand depends on the effiency of the CO_2 capture technologies.

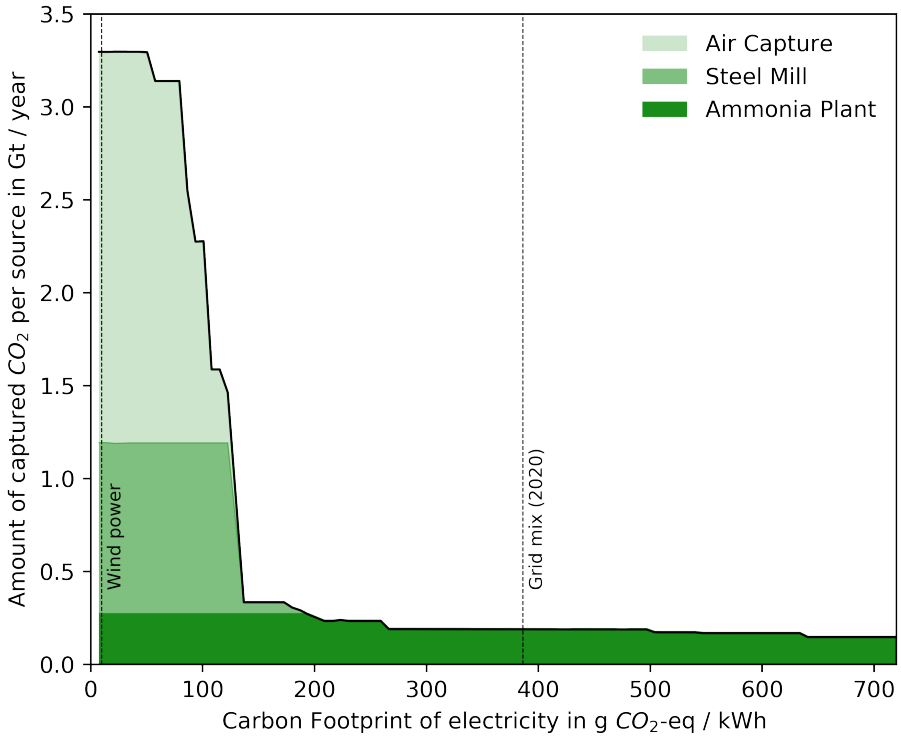

Figure 5.3.: Environmental merit-order curve for CO_2 supply from different sources. Wind: Electricity from wind power (9.57 g CO_2-eq/kWh). Grid mix (2020): Electricity from EU-28 grid mix (386 g CO_2-eq/kWh).

Figure 5.3 shows the amount of captured CO_2 per source. Over a wide range of electricity footprints, ammonia plants saturate the low CO_2 demand. At around 200 g CO_2-eq/kWh, we observe a sharp increase. More CCU technologies are applied, requiring more CO_2. As the carbon capture from ammonia plants is already depleted, the gap is filled by CO_2 from steel mills, precisely the steel mill off-gas separation system. Accordingly, the combustion of BFG/BOFG is decreased to recover CO_2 instead, as seen in Figure 5.2. However, the growing demand outruns both industrial point sources. Finally, direct air capture is applied to sastisfy the CO_2 demand of the chemical industry. For the best case scenario, the steel mill off-gas separation system accounts for 30 % of the supplied CO_2.

In the Appendix, we present the aggregated inputs and outputs of the optimal MGS for both electricity cases (Table D.1). The table accordingly represents a two-point discretization of the dynamic behavior observed in Figures 5.1 and 5.2. For a linear model, these discretization can be scaled and used as LCI processes. By switching between both processes, the dynamic behavior is approximated.

5.2. Optimal Process Design of the Separation System

Inputs and outputs of the optimal MGS change for different electricity scenarios. The optimal process design of the separation system is expected to change likewise, as the design has great influence on the output streams. For most separation and reaction steps, we include several unit alternatives in the superstructure (see Section 4.3). Furthermore, product recoveries and split factors are subject to the optimization. Each solution for the process design is characterized by the selection of units and the specification of unit variables. In the following section, we present process designs for the COG and the BFG/BOFG separation system. For each sub-system, we introduce the optimal design for two electricity scenarios. Then, we relate changes in the process design to changes in the overall system.

Table 5.1.: Optimal process design of the COG separation system for different scenarios. Best Case: Electricity from wind power (9.57 g CO_2-eq/kWh). Today: Electricity from EU-28 grid mix, 2020 (386 g CO_2-eq/kWh). ξ_{H_2} denotes the molar product recovery of hydrogen. $\xi^{\text{Reforming}}$ denotes the molar split factor of methane sent to the reforming unit.

	in 10^9	Today	Best case
H_2-Separation	-	**PSA**	**PSA**
ξ_{H_2}	-	0.899	0.927
Electricity	$\frac{MJ}{year}$	-78.1	-97.6
CH_4-Reforming	-	**CDR**	-
$\xi^{\text{Reforming}}$	-	0.14	0
Heat	$\frac{MJ}{year}$	-42.6	-
CO_2	$\frac{kg}{year}$	-6	-

Table 5.1 characterizes the process design of the COG separation system. In both cases, a PSA process performs H_2 separation consuming electricity. The product recovery, and respectively the electricity consumption, increase for the lower electricity carbon footprint. For today's electricity, the methane stream is partly sent to the reforming unit. There, SynGas is produced via CDR, with CO_2 as co-reactant. The endothermic CDR consumes heat. For best case electricity, the SynGas production discontinues. Two different reasons can explain the discontinuation: First, CCU technologies are significantly implemented for

the best case. Accordingly, the CO_2 demand rises and less efficient sources are exploited (see Figure 5.3). Competiting for CO_2 as resource, CDR seems less efficient than other CCU technologies. Second, the impact of electrical H_2 generation reduces, both for electrolysis and steel mill off-gas separation. Instead of CH_4 reforming, SynGas is produced by mixing H_2 and CO, obtained from electrolysis and steel mill off-gas separation, respectively.

Table 5.2.: Optimal process design of the BFG/BOFG separation system for different scenarios. Best case: Electricity from wind power (9.57 g CO_2-eq/kWh). Today: Electricity from EU-28 grid mix, 2020 (386 g CO_2-eq/kWh). ξ_k denotes the molar product recovery of component k. ξ^{WGSR} denotes the molar split factor of carbon monoxide sent to the water gas shift reactor.

	in 10^9	Today	Best case
CO-Separation	-	-	**TSA**
ξ_{CO}	-	-	0.9
Heat	$\frac{MJ}{year}$	0	-6250
ξ^{WGSR}	-	-	0.912
H_2O	$\frac{kg}{year}$	0	-205
CO_2-Separation	-	-	**PSA**
ξ_{CO_2}	-	-	0.882
Electricity	$\frac{MJ}{year}$	0	-1461
H_2-Separation	-	-	**PSA**
ξ_{H_2}	-	-	0.864
Electricity	$\frac{MJ}{year}$	0	-98

Table 5.2 shows the process design of the BFG/BOFG separation system. For today's electricity grid mix, combustion is preferred over separation (see Section 5.1). Accordingly, no BFG/BOFG separation system should be operated under this conditions. All following considerations on the optimal process design refer to the best case electricity scenario. The TSA process generates CO at maximum product recovery, consuming significant amounts of heat. However, most of the recovered CO is converted in the WGSR. With the use of heat and water, H_2 and CO_2 are produced. Subsequently, CO_2 is recovered at maximum rate. The electricity-driven PSA is preferred over the heat-driven CCA for this separation task. Lastly, another PSA step recovers H_2. Through this process design, the BFG/BOFG separation system aims on maximum CO_2 recovery.

5.3. Reduction Potential of the Polygeneration System

In the following section, we investigate the influence of steel mill off-gas separation on the GHG emissions of the steel and chemical industry. Figure 5.4 shows the cradle-to-grave emissions of the polygeneration system, thus the objective value, over the carbon footprint of electricity. Changes in the selected technologies cause bends in the curve. Through advancing electrification, the slope increases towards low electricity carbon footprints.

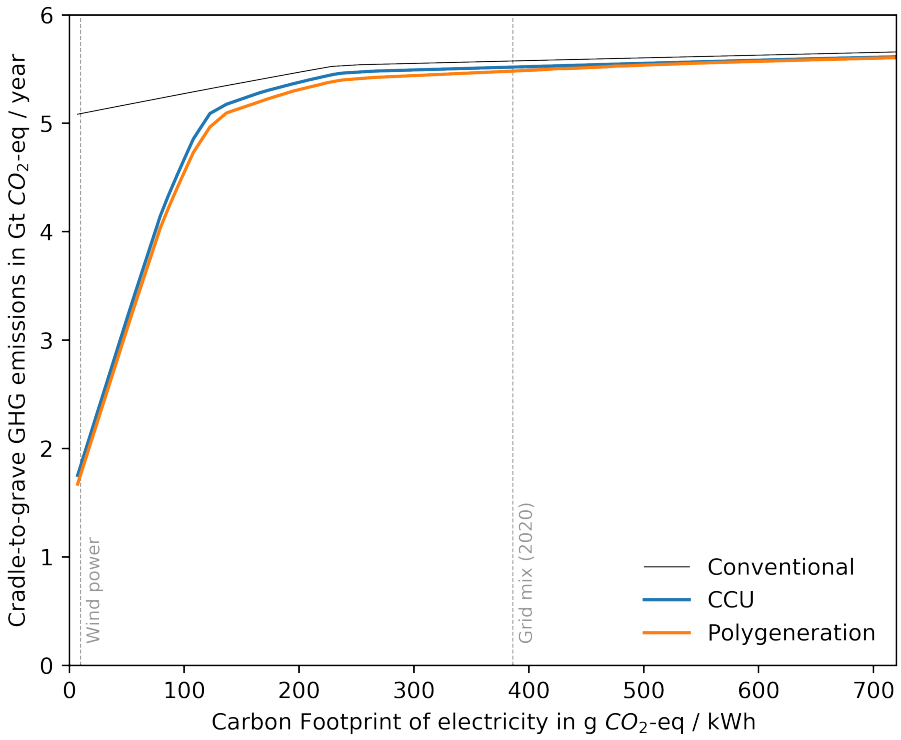

Figure 5.4.: GHG emissions of the steel and chemical industry over the carbon footprint of electricity. Conventional: Only conventional production processes, combustion of steel mill off-gases. CCU: Coventional or CCU production processes, combustion of steel mill off-gases. Polygeneration: Coventional or CCU production processes, combustion or separation of steel mill off-gases. Wind: Electricity from wind power (9.57 g CO_2-eq/kWh). Grid mix (2020): Electricity from EU-28 grid mix (386 g CO_2-eq/kWh).

In the conventional scenario, CCU and methanol-based processes are excluded from the model. Accordingly, all chemical products are produced by conventional processes. Steel mill off-gases are combusted in the CHP. We observe two technology changes: first, the application of power-to-heat at 232 g CO_2-eq/kWh, replacing combustion of natural gas; second, the application of water electrolysis to produce hydrogen at 202 g CO_2-eq/kWh. In the following, all GHG reduction potentials are referred to the conventional scenario.

In the CCU scenario, CCU and methanol-based processes are included in the model. Accordingly, chemical products can be produced by conventional or renewable processes. Steel mill off-gases are combusted in the CHP. In the polygeneration scenario, CCU and methanol-based processes are included in the model. Accordingly, chemical products can be produced by conventional or renewable processes. Steel mill off-gases are separated or combusted. Furthermore, we allow flexible combinations of both pathways.

We observe a slight decline in GHG emissions for decreasing electricity carbon footprints over 150 g CO_2-eq/kWh, similar for all three scenarios. For today's grid mix, the annual reduction potential through the use of CCU technologies amounts to 0.05 Gt CO_2-eq without the separation system, and 0.09 Gt CO_2-eq with the separation system. Below 150 g CO_2-eq/kWh, the decline accelerates significantly, if CCU technologies are enabled. Finally, the decrease sums up to the best-case reduction potential for electricity from wind power. The best-case reduction potential amounts to 3.26 Gt CO_2-eq per year without the separation system, and 3.34 Gt CO_2-eq per year with the separation system. Through flexible combinations of separation and combustion, the polygeneration system is able to meet or slightly undercut the CCU reference scenario at every point. However, the difference is almost neglectable on the scale of the overall GHG emissions. Performing steel mill off-gas separation influences neither the best-case reduction potential, nor the initial reduction slope in a significant way.

5.4. Discussion and Validation

The results indicate that the optimal design of the separation system strongly depends on the current electricity footprint. Thus, the implementation of such a system is subject to great uncertainty. Once the plant is constructed, changes in the design are difficult to conduct. Only one separation step is found eco-efficient for all investigated scenarios: The recovery of H_2 from COG via pressure swing adsorption. Accordingly, this technology should be prioritized for industrial implementation. Sustainable operation of a plant incorporates both environmental benefits and cost efficiency. However, in the present work, we use a strict environmental objective function. Future work should investigate, wether the presented system can be operated in a cost-efficient way.

Efficient CO_2 sources are required for the CCU-based production of chemicals. The separation of steel mill off-gases, in particular the BFG/BOFG stream, represents one possible source. With the presented merit-order curve (Figure 5.3), we can rank the CO_2 supply from steel mills in terms of environmental efficiency. For every explored scenario, the MGS performs better than direct air capture. Compared to ammonia plants, the CO_2 supply from the MGS is less efficient. This agrees with previous studies on CO_2 sources [28]. For every separation process, the feed product concentration is a crucial parameter. As CO_2 from ammonia plants is almost pure, the recovery is more energy efficient than from steel mill off-gases. Capturing the slight share of CO_2 in ambient air requires most energy of all investigated sources.

Kätelhön et al. [14] investigated the implementation of CCU technologies in the chemical industry, reporting a best-case GHG reduction potential of 3.4 Gt CO_2-eq per year. In the present study, we obtain a potential of 3.34 Gt CO_2-eq per year for the integrated model. Without the separation system, we obtain a potential of 3.26 Gt CO_2-eq per year. The accordance to the literature value validates the used model of the chemical industry. Main obstacle for the reduction of GHG emissions through CCU technologies is the dependency on low-carbon electricity: For today's grid mix, the reduction potential is insignificant. We observe, that steel mill off-gas separation does not mitigate this obstacle.

Convergence of the Integrated Model

Repetitive solving for different scenarios requires robustness and fast convergence of the model. For the linear TCM, we obtain solutions in split seconds through the use of state-of-the-art LP solvers. For integrated NLP or even MINLP/GDP sub-models, fastness and robustness of the solution decrease. We observed convergence problems for the integrated model, caused by certain unit operations. Unlike other considered reactors, the SMR reactor incorporates a two-step reaction network. Including this unit operation impairs the convergence of the overall model . The applied short-cut model for membrane processes (see Appendix B) represents a trade-off between product recovery and purity. Necesseraly, we set design specification constraints on the product purity. These constraints also impair the convergence of the overall model. Subsequently, we excluded MSP and SMR units from the flowsheet. The final model converges reasonable fast and robust, allowing repetitive solving to obtain the presented figures.

Validity of the MGS model

Unit operations for H_2 and CO_2 separation are well described in the literature. The selective CO separation is less investigated. We used a temperature swing adsorption process for this task, adapted from Ghanbari et al. [7]. Experimental data on the adsorption behaviour was obtained from Rabo et al. [22]. However, there is a lack of recent studies on the commercial implementation of this process.

In the applied superstructure, the by-product stream of the COG hydrogen separation is considered as CH_4. Due to this configuration, small amounts of other gases, in particular nitrogen, remain in the CH_4 stream. Dependig on the subsequent utilization, the purity of the CH_4 stream may be insufficient. To obtain better purities, another separation step could be included.

6. Summary and Conclusion

In the present study, we investigate the coupling of steel and chemical industry through steel mill off-gas separation. Recovered gas components can be used as feedstock for chemical production, thus reducing fossile fuel consumption and GHG emissions. However, the separation system requires energy, therefore causing indirect emissions. To capture the interactions between the sub-systems, we combine a detailed non-linear model of the separation system with a large-scale linear model of the chemical industry. The integrated model is optimized with an environmental objective function, representing the global warming impact.

The preferred utilization of steel mill off-gases, and hence the process design of the separation system, depend on the carbon footprint of electricity. Furthermore, the two steel mill off-gas streams, COG and BFG/BOFG, are treated differently. For today's grid mix, complete separation represents the optimal utilization for COG, producing hydrogen, methane and synthesis gas. Pressure swing adsorption and carbon dioxide reforming are applied to the separation system. The BFG/BOFG stream should be combusted to produce electricity and heat. For electricity from wind power, the production of SynGas from COG is decreased, recovering only hydrogen and methane. Separating the BFG/BOFG stream becomes environmentally beneficial, aiming on maximum CO_2 capture. For this separation step, the electricity-driven PSA is preferred over the heat-driven CCA. The separation system promotes CO_2-based production routes in the chemical industry, supplying up to 30% of the required CO_2. However, the reduction potential of steel mill off-gas separation is insignificant: While the implementation of CCU technologies without the separation system reduces GHG emissions by 3.26 Gt per year, the implementation of the separation system enables additional reduction of 80 Mt CO_2-eq per year.

In conclusion, the industrial implementation of the separation system underlies great uncertainty. The main drawback for utilizing CO_2 as feedstock, requiring large amounts of low-carbon electricity, is not mitigated by the polygeneration system. Furthermore, other technologies, including heat pumps and e-mobility, can use this low-carbon electricity more

efficient [15]. If and only if enough low-carbon electricity is available, we should implement carbon capture from steel mills and utilization in the chemical industry. The presented framework of extending the Technology Choice Model by a non-linear sub-model performs well on the case study, combining the advantages of both approaches: Robust modelling of a large-scale system and in-depth investigation of a smaller sub-system. The presented framework could be applied to future studies in this field.

Bibliography

[1] I. E. Agency. World energy outlook 2018, 2018.

[2] J. P. Birat. *Carbon dioxide (CO2) capture and storage technology in the iron and steel industry*, volume Carbon Dioxide (CO2) Capture, Transport and Industrial Applications, chapter 16, pages 492–521. Woodhead Publishing, 2010.

[3] Q. Chen, E. S. Johnson, J. D. Siirola, and I. H. Grossmann. Pyomo.gdp: Disjunctive models in python. *Computer Aided Chemical Engineering*, 44:889 – 894, 2018.

[4] W.-H. Chen, M.-R. Lin, T.-S. Leu, and S.-W. Du. An evaluation of hydrogen production from the perspective of using blast furnace gas and coke oven gas as feedstocks. *International Journal of Hydrogen Energy*, 36:11727 – 11737, 2011.

[5] F. Duchin and S. H. Levine. Sectors may use multiple technologies simultaneously: The rectangular choice-of-technology model with binding factor constraints. *Economic Systems Research*, 23(3):281 – 302, 2011.

[6] H. Ghanbari and H. Pettersson, Frank Saxen. Sustainable development of primary steelmaking under novel blast furnace operation and injection of different reducing agents. *Chemical Engineering Science*, 129:208 – 222, 2015.

[7] H. Ghanbari, H. Saxen, and I. E. Grossmann. Optimal design and operation of a steel plant integrated with a polygeneration system. *AIChE Journal*, 59(10):3659 – 3670, 2013.

[8] R. Goedecke. *Fluidverfahrenstechnik*. Wiley-VCH, 2006.

[9] I. E. Grossmann and F. Trespalacios. Systematic modeling of discrete-continuos optimization models through generalized disjunctive programming. *AIChE Journal*, 59(9):3276 – 3295, 2013.

[10] L. Gurobi Optimization. Gurobi optimizer reference manual, 2020.

[11] W. E. Hart, C. Laird, J.-P. Watson, and D. L. Woodruff. *Pyomo - Optimization Modeling in Python*. Springer, 2012.

[12] R. Heijungs and S. Suh. *The Computational Structure of Life Cycle Assessment*. Springer Science+Business Media, 2002.

[13] I. A. Kakavandi, E. J. Shokroo, and M. Baghbani. Dynamic modeling of nitrogen adsorption on zeolite 13x bed. *Fluid Mech Res Int*, 1:20 – 24, 2017.

[14] A. Kätelhön, A. Bardow, and S. Suh. Stochastic technology choice model for consequential life cycle assessment. *Environ. Sci. Technol.*, 50:12575 – 12583, 2016.

[15] A. Kätelhön, R. Meys, S. Deutz, S. Suh, and A. Bardow. Climate change mitigation potential of carbon capture and utilization in the chemical industry. *Proceedings of the National Academy of Sciences*, 116(23):11187–11194, 2019.

[16] H. Kim, J. Lee, S. Lee, I.-B. Lee, J.-h. Park, and J. Han. Economic process design for separation of co2 from the off-gas in ironmaking and steelmaking plants. *Energy*, 88:756 – 764, 2015.

[17] S. Kwon, M. Fan, H. F. M. DaCosta, A. G. Russell, K. A. Berchtold, and M. K. Dubey. Co2 sorption. In D. A. Bell, B. F. Towler, and M. Fan, editors, *Coal Gasification and Its Applications*, chapter 10. Elsevier, 2010.

[18] J. A. Lie, T. Vassbotn, M.-B. Hägg, D. Grainger, T.-J. Kim, and T. Mejdell. Optimization of a membrane process for co2 capture in the steelmaking industry. *International Journal of Greenhouse Gas Control*, 1:309 – 317, 2007.

[19] P. Linstrom and W. Mallard. *NIST Chemistry WebBook, NIST Standard Reference Database Number 69*. National Institute of Standards and Technology, Gaithersburg MD, 20899, 2020.

[20] L. Mencarelli, Q. Chen, A. Pagot, and I. E. Grossmann. A review on superstructure optimization approaches in process system engineering. *Computers & Chemical Engineering*, 136, 2020.

[21] R. Notz, I. Tönnies, H. P. Mangalapally, S. Hoch, and H. Hasse. A short-cut method for assessing absorbents for post-combustion carbon dioxide capture. *International Journal of Greenhouse Gas Control*, 5:413 – 421, 2010.

[22] J. A. Rabo, J. N. Francis, and C. L. Angell. Selective adsorption of carbon monoxide from gas streams. United States Patent 4019879, 1977.

[23] R. Raman and I. H. Grossmann. Modelling and computional techniques for logic based integer programming. *Computers chem. Engng*, 18(7):563 – 578, 1994.

[24] D. M. Ruthven, S. Farooq, and K. S. Knaebel. *Pressure Swing Adsorption*. Wiley-VCH, 1994.

[25] P. Styring, E. A. Quadrelli, and K. Armstrong. *Carbon Dioxide Utilisation: Closing the Carbon Cycle*. Elsevier, 2014.

[26] M. Türkay and I. H. Grossmann. Logic-based minlp algorithms for the optimal synthesis of process networks. *Computers chem. Engng*, 20(8):959 – 978, 1996.

[27] W. Uribe-Soto, J.-F. Portha, J.-M. Commenge, and L. Falk. A review of thermochemical processes and technologies to use steelwork off-gases. *Renewable and Sustainable Energy Reviews*, 74:809 – 823, 2017.

[28] N. von der Assen, , L. J. Muller, A. Steingrube, P. Voll, and A. Bardow. Selecting co2 sources for co2 utilization by environmental-merit-order curves. *Environ. Sci. Technol.*, 50:1093–1101, 2016.

[29] N. von der Assen, P. Voll, M. Peters, and A. Bardow. Life cycle assessment of co2 capture and utilization: a tutorial review. *Chem. Soc. Rev.*, 43:7982–7994, 2014.

[30] A. Wächter and L. T. Biegler. On the implementation of an interior-point filter line-search algorithm for large-scale nonlinear programming. *Math. Program.*, 106:25 – 57, 2006.

[31] S. Wang, G. Q. Lu, and G. J. Millar. Carbon dioxide reforming of methane to produce synthesis gas over metal-supported catalysts: State of the art. *Energy and Fuels*, 10:896 – 904, 1996.

[32] G. Wernet, C. Bauer, B. Streubing, E. Moreno-Ruiz, and B. Weidema. The ecoinvent database version 3 (part i): overview and methodology. *The International Journal of Life Cycle Assessment*, 21:1218 – 1230, 2016.

[33] J. Zhu, D. Zhang, and K. D. King. Reforming of ch4 by partial oxidation: thermodynamic and kinetic analyses. *Fuel*, 80:899 – 905, 2001.

A. List of Abbreviations and Symbols Used

List of Abbreviations

BFG	Blast Furnace Gas
BOFG	Basic Oxygen Furnace Gas
CCA	Carbon Chemical Absorption
CCU	Carbon Capture and Utilization
CDR	Carbon Dioxide Reforming (of Methane)
CHP	Combined Heat and Power Unit
COG	Coke Oven Gas
GDP	Generalized disjunctive (optimization) program
GHG	Green House Gas
GWI	Global Warming Impact
LCA	Life Cycle Assessment
LCI	Life Cycle Inventory
LP	Linear (optimization) program
LTSR	Low Temperature Shift Reaction
MEA	Monoethanolamine
MGS	Steel Mill Off-Gas Separation
MINLP	Mixed-integer non-linear (optimization) program
MIP	Mixed-integer linear (optimization) program
MSP	Membrane Separation Process

NLP	Non-linear (optimization) program
POR	Partial Oxygen Reforming (of Methane)
PSA	Pressure Swing Adsorption
SMR	Steam Methane Reforming
TCM	Technology Choice Model
TRL	Technology Readiness Level
TSA	Temperature Swing Adsorption

List of Symbols

α	Membrane selectivity	$[-]$
β	Adsorbent selectivity	$[-]$
ΔH_R	Reaction enthalpy	$\left[\frac{kJ}{mol}\right]$
η	Efficiency	$[-]$
κ	Molar heat capacity ratio	$[-]$
ν	Stoichionetric coefficient	$[-]$
ξ	Conversion rate	$[-]$
ζ^i	Split factor	$[-]$
ζ_k	Product recovery	$[-]$
A	Technology matrix	$[-]$
B	Environmental flow matrix matrix	$[-]$
c_i	Connector	$[-]$
C_p	Molar heat capacity	$\left[\frac{kJ}{molK}\right]$
c_p	Specific heat capacity	$\left[\frac{kJ}{kgK}\right]$
h	Impact vector	$[-]$
h	Molar enthalpy	$\left[\frac{kJ}{mol}\right]$
M	Molar weight	$\left[\frac{kg}{mol}\right]$

n^i	Molar flow	$\left[\frac{mol}{year}\right]$
p	Pressure	$[bar]$
p_i	Production volume	$[-]$
Q	Characterization matrix	$[-]$
q	Heat flow	$\left[\frac{MJ}{year}\right]$
R	Gas constant	$\left[\frac{kJ}{molK}\right]$
s	Scaling vector	$[-]$
s_j	Scaling factor	$[-]$
T	Temperature	$[K]$
t	Temperature	$[°C]$
v	End-of-life vector	$[-]$
w	Electricity flow	$\left[\frac{MJ}{year}\right]$
X	Mass loading	$[-]$
y_k^i	Mole fraction (gas)	$[-]$
y_i	Final demand	$[-]$

List of indices (superscript)

i	Stream i in separation system
in	Input stream
lean	Lean solvent stream
out	Output stream
prod	Product stream
rich	Rich solvent stream

List of indices (subscript)

i	Intermediate flow i in TCM
j	Process j in TCM

k	Chemical component k
abs	Absorber
ads	Adsorber
des	Desorber
key	Key component
prod	Product component

B. Model Equations and Parameters

In the following chapter, a list of equations and parameters used for the separation system is presented.

Heat Exchanger and Compressor

Energy demands for heat exchangers and compressors are calculated by energy balances:

$$q_{\mathsf{HE}} = n^{\mathsf{in}}(h^{\mathsf{out}} - h^{\mathsf{in}})/\eta_{\mathsf{HE}} \tag{B.1}$$

$$w_{\mathsf{comp}} = n^{\mathsf{in}}(h^{\mathsf{out}} - h^{\mathsf{in}})/\eta_{\mathsf{comp}} \tag{B.2}$$

The efficiencies are set to $\eta_{\mathsf{comp}} = 0.7$ and $\eta_{\mathsf{HE}} = 0.7$

Thermodynamical Properties

Pure substance enthalpies for all mill gas components are estimated by the shomate equation:

$$h_k(T) = B_{1k} + B_{2k}\frac{T^2}{2} + B_{3k}\frac{T^3}{3} + B_{4k}\frac{T^4}{4} - \frac{B_{5k}}{T} + B_{6k} - B_{7k} \tag{B.3}$$

Coefficients B_{1k} - B_{7k} are obtained from the NIST chemical webbook [19].

Enthalpy of each stream is calculated under assumption of an ideal gas mixture:

$$h^i = \sum_k h_k(T^i) y_k^i \tag{B.4}$$

Isentropic relation for ideal gas:

$$\frac{T^{\mathsf{out}}}{T^{\mathsf{in}}} = \frac{p^{\mathsf{out}}}{p^{\mathsf{in}}}^{\frac{\kappa-1}{\kappa}} \tag{B.5}$$

with heat capacity ratio κ and gas constant R:

$$\kappa = \frac{C_p}{C_p - R} \tag{B.6}$$

The molar heat capacities C_p are calculated with the derivative of the shomate equation B.3.

Pressure Swing Adsorption

Following shortcut equation is used to calculate the product recovery with respect to the pressure ratio. The adsorbent selectivity is denoted by β [24]:

$$\frac{p^{\text{prod}}}{p^{\text{in}}} = y^{\text{in}}_{k_{\text{prod}}} \left(1 - \frac{\zeta_{k_{\text{prod}}}}{1 - \beta}\right) \tag{B.7}$$

For hydrogen recovery ($k_{\text{prod}} = H_2$), a selectivity of $\beta_{H_2} = 0.02$ is used [7].

For carbon dioxide recovery ($k_{\text{prod}} = CO_2$), equation B.7 was fitted to operational data from Kim et al. [16], resulting in $\beta_{CO_2} = 0.024$.

The product stream is assumed to be pure target component ($y^{\text{prod}}_{k_{\text{prod}}} = 1$).

Temperature Swing Adsorption

Similar to the PSA, the product stream is assumed as pure target component.

Through a mass balance with adsorbent stream m_{ads}, the product flow is determined. X^{rich} and X^{lean} denote rich and lean adsorbent mass loadings.

$$m_{\text{ads}}(X^{\text{rich}} - X^{\text{lean}}) = M_{CO}\, n^{\text{prod}} y^{\text{prod}}_{CO} \tag{B.8}$$

As main energy requirement, the desorption heat q_{des} is calculated. Because of very small loadings, adsorption enthalpy and product heating are neglected.

$$q_{\text{des}} = m_{\text{ads}} c_{p,\text{ads}} (t_{\text{des}} - t_{\text{ads}}) \tag{B.9}$$

Adsoprtion isotherms from Rabo et al. [22] at $t_{\text{ads}} = 50°\text{C}$ and $t_{\text{des}} = 250°\text{C}$ are used to determine rich and lean loadings.

The adsorbent (zeolite 13X) heat capacity $c_{p,\text{ads}}$ was obtained from [13].

Carbon Chemical Absorption

The desorption heat for the chemical absorption process of CO_2 with MEA is estimated with an empirical correlation from Kim et al. [16]:

$$q = 4.2 n^{\text{prod}} M_{CO_2} \tag{B.10}$$

The product recovery is constrained by $\zeta_{CO_2} \leq 0.9$. The process is operated at fixed temperatures $t_{\text{des}} = 120°C$ and $t_{abs} = 40°C$ and and a pressure of 1.5 bar.

A more advanced shortcut model by Notz et al. [21], based on the Kremser equation, was also tested but seemed to impair overall convergence.

Membrane Separation Process

The shortcut equations for the MSP are adapted from [7].

Product recovery:

$$\frac{p^{\text{prod}}}{p^{\text{in}}} = \left(\frac{y^{\text{in}}_{k_{\text{prod}}}}{y^{\text{prod}}_{k_{\text{prod}}}} \right) \left(\frac{1 - \zeta_{k_{\text{prod}}}}{1 - y^{\text{in}}_{k_{\text{prod}}} \zeta_{k_{\text{prod}}}} \right) \tag{B.11}$$

Mole fraction of k in the product stream:

$$n^{\text{prod}} y^{\text{prod}}_k = \frac{\alpha_{k/k_{\text{prod}}} \zeta_{k_{\text{prod}}} y^{\text{in}}_k y^{\text{in}}_{k_{\text{prod}}} n^{\text{in}}}{y^{\text{in}}_k \left(2 - \zeta_{k_{\text{prod}}} - \frac{\alpha_{k/k_{\text{prod}}} \zeta_{k_{\text{prod}}}}{1 - y^{\text{in}}_{k_{\text{prod}}} \zeta_{k_{\text{prod}}}} \right) - 2 \left(\frac{y^{\text{prod}}_{k_{\text{prod}}} p^{\text{in}}}{p^{\text{prod}}} \right) (1 - \alpha_{k/k_{\text{prod}}})} \tag{B.12}$$

The membrane selectivities $\alpha_{k/k_{\text{prod}}}$ for the H_2 separation are obtained from [7], for the CO_2 separation from [18].

Chemical Reactions

For a chemical reaction R, $\nu_{k,R}$ denotes the stoichiometric coefficient of component k. The conversion rate ξ_R is determined on basis of the limiting key component k_{key}.

Overall mole balance:

$$n^{\text{in}}(1 + \sum_{k} \nu_{k,R} \xi_R y^{\text{in}}_{k_{\text{key}}}) = n^{\text{out}} \tag{B.13}$$

Component mole balance:

$$n^{\text{in}}(y^{\text{in}}_k - \frac{\nu_{R,k}}{\nu_{R,k_{\text{key}}}} \xi_R y^{\text{in}}_{k_{\text{key}}}) = n^{\text{out}} y^{\text{out}}_k \tag{B.14}$$

Energy balance with enthalpy of reaction ΔH_R:

$$n^{\text{in}}(h^{\text{in}} - \xi_R y^{\text{in}}_{k_{\text{key}}} \Delta H_R) + q\eta_{\text{HE}} = n^{\text{out}} h^{\text{out}} \tag{B.15}$$

The occuring reactions are modelled with fixed conversion rates and reaction temperatures. These parameters can be found in table B.1. $\frac{n_{k_s}}{n_{k_{\text{key}}}}$ denotes the ratio of supplemented co-reactant k_s to key component in the feed stream.

Concurrent to the SMR at its operating condition, the WGSR reaction takes place with $\xi_{CO}^{WGSR} = 0.4$.

Table B.1.: Reaction parameters of the separation system

Reaction	ΔH_R in kJ/mol	T_R in K	k_{key}	$\xi_{k_{\text{key}}}$	k_s	$\frac{n_{k_s}}{n_{k_{\text{key}}}}$
WGSR	-41.1	473 - 573	CO	0.96	H_2O	1
SMR	234.7	1153 - 1300	CH_4	0.82	H_2O	3.68
POR	-35.9	1000	CH_4	0.95	O_2	0.48
CDR	247	1143 - 1313	CH_4	0.9	CO_2	1

C. Production Volumes of the Chemical Industry

Table C.1.: Production volumes p_i of the considered chemical products

Product i	p_i in $Mt/year$	Product i	p_i in $Mt/year$
1,3-propanediol	0.146	Isobutyralaldehyde	1.000
1,4-butanediol	2.000	Methanol	134.500
2-ethylhexanol	0.004	Methyl formate	0.002
Acetic acid	13.000	Methyl methacrylate	3.500
Acetone	6.700	n-butanol	3.800
Acetaldehyde	2.000	n-butyraldehyde	7.000
Acetylene	0.400	Octene	0.609
Acrylic acid	5.850	Phenol	17.400
Acrylonitril	10.400	Phosgene	6.000
Ammonia	228.900	Polycarbonate	4.100
Benzene	66.000	Polyethylene	163.194
Calcium formate	0.695	Polyol	7.500
Caprolactam	3.480	Polypropylene	100.706
Cumene	24.300	Propylene	139.175
Cyclohexane	9.190	Propylene Oxide	13.900
Dimethyl carbonate	0.090	Styrene	48.600
Diphenyl carbonate	0.254	Terephthalic acid	100.690
Ethylbenzene	37.000	Toluol	34.700
Ethylene	250.000	Toluene diisocyanate	3.360
Ethylene glycol	41.700	Urea	197.000
Ethylene oxide	41.700	Vinyl acetate	6.970
Formic acid	0.708	Vinyl chloride	55.600
Formaldehyde	20.900	Xylene (mixed)	93.700
Isobutanol	0.552	Xylene (para)	69.500
Isobutylene	15.000		

D. Annual Inputs and Outputs of the Separation System

Table D.1.: Annual inputs and outputs of the separation system for different scenarios. Best Case: Electricity from wind power (9.57 g CO_2-eq/kWh). Today: Electricity from EU-28 grid mix, 2020 (386 g CO_2-eq/kWh). The GWI of the separation system is related to unrecovered CO and CO_2 shares in purge streams.

Interm. Flow	in 10^9	Today	Best case
CO_2	kg	-6	918
CO	kg	0	31
Electricity	MJ	-78.1	-1559
Heat	MJ	-62.8	-5469
H_2	kg	4.9	28
CH_4	kg	13.5	16
BFG / BOFG	kg	0	-1740
COG	kg	-39.7	-39.7
Steam	kg	0	-204.9
SynGas 1:1	kg	9.8	0
GWI	kg CO_2-eq	0	203.5